Study of Gamow-Teller transitions in isotopes of titanium within the quasi particle random phase approximation

Sadiye Cakmak [1,2], Jameel-Un Nabi [2], Tahsin Babacan [1] and Cevad Selam [3]

Abstract The Gamow-Teller (GT) transition is inarguably one of the most important nuclear weak transitions of the spin-isosopin $\sigma\tau$ type. It has many applications in nuclear and astrophysics. These include, but are not limited to, r-process β-decays, stellar electron captures, neutrino cooling rates, neutrino absorption and inelastic scattering on nuclei. The quasiparticle random phase approximation (QRPA) is an efficient way to generate GT strength distribution. In order to better understand both theoretical systematics and uncertainties, we compare the GT strength distributions, centroid and width calculations for $^{40-60}$Ti isotopes, using the pn-QRPA, Pyatov method (PM) and the Schematic model (SM). The pn-QRPA and SM are further sub-divided into three categories in order to highlight the role of particle-particle (pp) force and deformation of the nucleus in the GT strength calculations. In PM, we study only the influence of the pp force in the calculation. We also compare with experimental results and other calculations where available. We found that the inclusion of pp force and deformation significantly improves the performance of SM and pn-QRPA models. Incorporation of pp force leads to pinning down the centroid value in the PM. The calculated GT strength functions using the pn-QRPA (C) and SM (C) models are in reasonable agreement with measured data.

Sadiye Cakmak , Jameel-Un Nabi , Tahsin Babacan and Cevad Selam

[1]Department of Physics, Celal Bayar University, Manisa, Turkey

[2]Faculty of Engineering Sciences, GIK Institute of Engineering Sciences and Technology, Topi 23640, Swabi, Khyber Pakhtunkhwa, Pakistan

[3]Department of Physics, Alparslan University, Mus, Turkey

This study is supported by BAP project of Celal Bayar University with number 2013-004

Keywords pn-QRPA; Pyatov method; Schematic model; GT strength distributions (total GT strengths, centroids, widths); Ikeda sum rule; titanium isotopes

1 Introduction

The Gamow-Teller (GT) response of nuclei in the medium mass region are crucial prerequisites in order to determine the precollapse evolution of a supernova (1). GT excitations act only on the spin-isospin ($\sigma\tau$) degrees of freedom. The isospin operator in spherical coordinates has three components $\tau_{\pm,0}$. Here, the plus sign refers to Gamow-Teller (GT_+) transitions in which a proton is changed into a neutron (e.g. in β^+ decays and electron captures), while the minus sign corresponds to GT_- transitions in which a neutron is changed into a proton (realized in β^--decays). The total GT_- and GT_+ strengths, noted as S_- and S_+, respectively, are connected by the model independent Ikeda sum rule as $S_- - S_+ = 3(N - Z)$, where N and Z are the numbers of neutrons and protons (2). The third component GT_0 is of relevance to inelastic neutrino-nucleus scattering for low neutrino energies and it would not be further considered in this manuscript. The GT transitions in fp-shell nuclei play decisive roles in presupernova phases of massive stars and also during the core collapse stages of supernovae, specially in neutrino induced processes. The lepton fraction (Y_e) of the stellar matter is one of the factors that controls the gravitational core-collapse of massive stars. It is the degeneracy pressure of the leptons which counters the mammoth gravitational force of massive stars. Once the lepton contents of the stellar matter reduce, the core collapses within fractions of a second. The lepton content of the stellar matter in turn is governed by β-decay and electron capture rates among iron-regime nuclides. The β-decay gives positive contribution whereas electron capture rates give a negative contribution to Y_e. The time

evolution of Y_e is a crucial parameter which is also a key to generate a successful explosion in modeling and simulation of core-collapse supernovae. Nuclei in the mass range A $\sim$ 60, at stellar densities less than around 10^{11} gcm^{-3}, posses electron chemical potential of the same order of magnitude as the nuclear Q-value. Under such conditions the electron capture rates are sensitive to the detailed GT distributions. A reliable and microscopic calculation of ground and excited states GT distribution functions is then in order. At much higher stellar densities, the electron chemical potential is much larger than Q-values. For high densities electron capture rates are more sensitive to the total GT strength. Additionally for higher densities centroids and widths of the GT distribution become important parameters for estimation of weak-interaction rates. Hence one needs not only the microscopic GT strength distribution functions but also the total strength, centroid and width of the distributions to reliably calculate electron capture rates in stellar matter under given physical conditions.

GT distributions have been extracted experimentally using different techniques. The isovector response of nuclei may be studied using the nucleon charge-exchange reactions (p, n) (e.g. (3)) or (n, p) (e.g. (4)); by other reactions such as (^{3}He,t) (e.g. (5)) or (t,^{3}He) (e.g. (6)), (d,^{2}He) (e.g. (7)) or through heavy ion reactions (e.g. (8)). The GT cross sections ($\Delta T = 1, \Delta S = 1, \Delta L = 0$, $0\hbar\omega$ excitations) are proportional to the analogous beta-decay strengths at vanishing linear momentum transfer. Charge-exchange reactions at small momentum transfer can therefore be used to study beta-decay strength distributions when beta-decay is not energetically possible. The (p, n), (^{3}He,t) reactions probe the GT$_-$ strength whereas the (n, p), (d,^{2}He) reactions give the GT$_+$ strength.

One also requires GT strength distributions of hundreds of unstable nuclei which requires much effort and technology to be studied experimentally. The situation is improving with the construction of next-generation radioactive ion-beam facilities. To further complicate the matters, one also requires excited state GT strength distribution functions in astrophysical environments (as parent excited states are thermally populated at high stellar temperatures) where no measured data is available. Consequently, astrophysical calculations rely heavily on detailed microscopic calculations.

Theoretical calculations of GT transitions fall generally into three major categories: simple independent-particle models; full-scale interacting shell-model calculations; and, in between, the random-phase approximation (RPA) and quasi-particle random-phase approximation (QRPA). The simple independent-particle models have reported to pose problems in correct placement of GT centroid. These models place the centroid of the GT strength too high for even-even parent nuclides and too low on odd-A and odd-odd parents (9). Full interacting shell-model calculations are computationally demanding although one can exploit the Lanczos algorithm to efficiently generate the strength distribution (10). For medium-mass nuclei, one still needs to choose from among a number of competing semi-realistic/semi-empirical interactions in shell model calculations. RPA and QRPA can be treated as approximations to a full shell-model calculation and they are much less demanding computationally. Furthermore, they have the additional advantage that one can employ a separable multi-shell interaction which in turn grant access to a huge model space, up to $7\hbar\omega$, to perform the calculations.

The main difficulty with both experiment and theory is that the strength distribution connects to many states. In contrast to Fermi transitions, which relate a parent state to a single daughter state (the isobaric analog state), GT transitions are fragmented over many daughter states. This is caused by the fact that the GT operator does not commute with the residual interaction beyond the mean-field approximation which gives rise to shell model single-particle orbits.

Three widely used model within the QRPA formalism are the pn-QRPA model, the Schematic Model (SM) and the Pyatov Method (PM). The pn-QRPA theory is an efficient way to generate GT strength distributions. It was Halbleib and Sorenson (11) who generalized this model to describe charge-changing transitions of the type $(Z, N) \rightarrow (Z \pm 1, N \mp 1)$ whereas the usual RPA was formulated for excitations in the same nucleus. The model was then extended from spherical to deformed nuclei (using Nilsson-model wave functions) by Krumlinde and Möller (12). Further extension of the model to treat odd-odd nuclei and transitions from nuclear excited states was done by Muto and collaborators (13). It was Nabi and Klapdor-Kleingrothaus who used the pn-QRPA theory for the first time to calculate the stellar weak interaction rates over a wide range of temperature and density scale for sd- (14) and fp/fpg-shell nuclei (15) in stellar matter (see also Ref. (16)). Since then, these calculations were further refined with use of more efficient algorithms, computing power, incorporation of latest data from mass compilations and experimental values, and fine-tuning of model parameters (e.g. see (17; 18; 19; 20; 21; 22; 23; 24)). There is a considerable amount of uncertainty involved in all types of calculations of stellar weak interactions. The uncertainty associated with the microscopic calculation of the pn-QRPA model was discussed in detail in Ref. (19). The reliability of the pn-QRPA calculations was discussed in length by Nabi and Klapdor-Kleingrothaus

(15). There, the authors compared the measured data (half lives and B($GT_{\pm}$) strength) of thousands of nuclide with the pn-QRPA calculations and got fairly good comparison.

The formalism developed by Pyatov (25) has been applied to different problems for more than 35 years. The main step of Pyatov formalism is based on the definition of the effective Hamiltonian which considers Dirac restrictions (26). This formalism has been used in problems which include the violation of the particle number (27), invariant invariance (28), generalized Galielo invariance (29) and velocity dependent effect (30). Moreover, this formalism has also been applied by Civitarese et. al. (31) to the isospin dependent Hamiltonians in quasi-particle basis in order to investigate the relation between the collapse of RPA solutions and the violation of isospin symmetry. It has also been used by Magierski and Wyss (32). In studies done by Kuliev and collaborators (33) and Babacan et. al. (34; 35; 36), this method was applied to scissor mode vibrations, isobar analog states (IAS) and isospin admixtures in the ground states of spherical nuclei as well as Gamow-Teller Resonance (GTR) states. Coherent excitation of the nucleons results in concentration of most of total GT transition strength in a narrow excitation region in the daughter nucleus known as GTR states. These resonances correspond to the coherent proton-hole proton and neutron-hole neutron excitations in the known electromagnetic giant resonances. Schematic Model is a special case of Pyatov method and it would be discussed further in the next section.

Weak rates on titanium isotopes have numerous astrophysical applications. The estimated ^{44}Ti yield from post explosive nucleosynthesis supernova debris can be given as an example and it can be used to test and calibrate the supernova models (37). β-decay of ^{40,41}Ti has implications for solar-neutrino detection (38). The large energy release of the ^{40}Ti decay [$Q_{ec} = 11680(160)$ KeV] enables one to extract all information that is relevant for the GT contribution to the rate of solar neutrinos absorbed by ^{40}Ar. Titanium isotopes have been assigned different nucleosynthetic origins. Oxygen burning for ^{46}Ti, silicon and carbon burning for ^{47,49}Ti, silicon burning for the abundant isotope ^{48}Ti, and carbon burning for ^{50}Ti. The difference in these origins helps us to explain the life time of the Galaxy and its gradual evolution (18). Aufderheide and collaborators (39) searched for key weak interaction nuclei in presupernova evolution. Phases of evolution in massive stars, after core silicon burning, were considered and a search was performed for the most important electron captures and β-decay nuclei in these scenarios. From these lists, electron captures on ^{49,51,52,53,54}Ti and β-decay of ^{51,52,53,54,55,56}Ti were short-listed to be of astrophysical importance. Again, per simulation results of Heger and collaborators (40), weak rates on isotopes of titanium are considered as very important for presupernova evolution of massive stars.

In this paper, we calculate and compare GT strength distributions of isotopes of titanium (mass number 40 to 60) using three different (microscopic) QRPA models namely pn-QRPA, Pyatov Method (PM) and the Schematic Model (SM). All three models are further divided into two sub-categories:
(A) Nuclei are treated as spherical and only particle-hole (ph) interaction is taken into account. The resulting model is referred to as Model (A) in this manuscript.
(B) The particle-particle interaction is usually thought to play a minor role in β^- decay but has shown to be of decisive importance in β^+ decay and electron capture reactions (41) in pn-QRPA models. Particle-particle (pp) interaction is then incorporated into the Model (A) to get our Model (B).

The pn-QRPA and SM are further classified into a third category in order to study the effect of deformation of nucleus on the GT strength functions. The deformation parameter is recently argued to be one of the most important parameters in pn-QRPA calculations (42). In order to check the effect of incorporation of deformation in the pn-QRPA and SM models, we finally lift the initial assumption of spherical nuclei and introduce deformations in the Model (B) to get Model (C). In other words, Model (C) takes into account nuclear deformations and also perform calculation in *both* pp *and* ph channels. Incorporation of deformation into PM is currently being worked on and it would be taken up as a future assignment.

The next section briefly describes the theoretical formalism used to calculate the GT strength distributions using the PM, SM and the pn-QRPA theory. The calculated $GT_{\pm}$ strength distributions for titanium isotopes are presented and compared with measurements and against other theoretical calculations in Sec. 3. The main conclusions of this work are finally presented in Sec. 4.

2 Theoretical Formalism

2.1 Pyatov Method and the Schematic Model

Restoration of the broken super symmetry property in static pairing interaction potential is of great importance for GT transitions. On the other hand, no effect of the translational and rotational invariance violations

on GT transitions is seen. The Pyatov Method (PM) used in this paper provides this restoration in two different ways: addition of static interaction potential to the total Hamiltonian after its broken symmetry property has been restored and the restoration of the broken symmetry in quasi particle space. We employ the second method in this article. The Schematic Model (SM) is a special case of the PM where we exclude the effective interaction term from the total Hamiltonian. We next consider the case of even-even and odd-A cases separately and describe the necessary formalism within the PM and SM.

2.1.1 Even-Even Nuclei

The Schematic Model (SM) Hamiltonian for GT excitations in the quasi particle representation is given as

$$H_{SM} = H_{SQP} + h_{ph} + h_{pp}, \quad (1)$$

where H_{SQP} is the Single Quasi Particle (SQP) Hamiltonian, h_{ph}^{GT} and h_{pp}^{GT} are the GT effective interactions in the ph and pp channels, respectively (43). The effective interaction constants in the ph and pp channel were fixed from the experimental value of the Gamow-Teller resonance (GTR) energy and the β-decay *logft* values between the low energy states of the parent and daughter nucleus, respectively. In order to restore the super symmetry property of the pairing part in total Hamiltonian, certain terms which do not commute with the GT operator were excluded from total Hamiltonian and the broken commutativity of the remaining part due to the shell model mean field approximation was restored by adding an effective interaction term h_0

$$[H_{SM} - h_{ph}^{GT} - h_{pp}^{GT} - V_1 - V_c - V_{ls} + h_0, G_{1\mu}^{\pm}] = 0, \quad (2)$$

or

$$[H_{SQP} - V_1 - V_c - V_{ls} + h_0, G_{1\mu}^{\pm}] = 0, \quad (3)$$

where V_1, V_c and V_{ls} are isovectors, Coulomb and spin orbital term of the shell model potential, respectively. The restoration term h_0 in Eq. (3) is included in a separable form:

$$h_0 = \sum_{\rho=\pm} \frac{1}{2\gamma_\rho} \sum_{\mu=0,\pm1} [H_{sqp} - V_c - V_{ls} - V_1, G_{1\mu}^{\rho}]^{\dagger} \cdot$$

$$[H_{sqp} - V_c - V_{ls} - V_1, G_{1\mu}^{\rho}]. \quad (4)$$

The strength parameter γ_ρ of h_0 effective interaction is found from the commutation condition in Eq. (3) and the following expression is obtained for this constant (for details see Ref. (44)).

$$\gamma_\rho = \frac{\rho}{2} \langle 0 | [[H_{sqp} - V_c - V_{ls} - V_1, G_{1\mu}^{\rho}], G_{1\mu}^{\rho}] | 0 \rangle.$$

The total Hamiltonian of the system according to PM finally becomes

$$H_{PM} = H_{SQP} + h_0 + h_{ph} + h_{pp}. \quad (5)$$

The eigenvalues and eigenfunctions of Hamiltonian given in Eq. (5) are solved within the framework of the pn-QRPA method. We considered the GT 1^+ excitations in odd-odd nuclei generated from the correlated ground state of the parent nucleus by the charge-exchange spin-spin forces and used the eigenstates of the single quasi particle Hamiltonian H_{SQP} as a basis.

In pn-QRPA, the i^{th} excited GT 1^+ states in odd-odd nuclei are considered as the phonon excitations and described by

$$|1_i^+ > = Q_i^{\dagger}(\mu)|0 >$$

$$= \sum_{np} [\psi_{np}^i C_{np}^{\dagger}(\mu) - (-1)^{1+\mu} \varphi_{np}^i C_{np}(-\mu)]|0 >, \quad (6)$$

where $Q_i^{\dagger}(\mu)$ is the pn-QRPA phonon creation operator, $|0>$ is the phonon vacuum which corresponds to the ground state of an even-even nucleus and fulfills $Q_i(\mu)|0 >= 0$ for all i. The ψ_{np}^i and φ_{np}^i are quasi boson amplitudes.

Assuming that the phonon operators obey the commutation relations

$$< 0|[Q_i(\mu), Q_j^{\dagger}(\mu')]|0 >= \delta_{ij}\delta_{\mu\mu'},$$

we obtain the following orthonormalization condition for amplitudes ψ_{np}^i and φ_{np}^i

$$\sum_{np} [\psi_{np}^i \psi_{np}^{i'} - \varphi_{np}^i \varphi_{np}^{i'}] = \delta_{ii'}. \quad (7)$$

The energies and wave functions of the GT 1^+ states are obtained from the pn-QRPA equation of motion:

$$[H_{PM}, Q_i^{\dagger}(\mu)]|0 >= \omega_i Q_i^{\dagger}(\mu)|0 >, \quad (8)$$

where ω_i is the energy of the GT 1^+ states occurring in neighboring odd-odd nuclei. We obtain the secular equation for excitation energies ω_i of the GT 1^+ states in the neighbor odd-odd nuclei:

$$[\chi_+ - \sum_{np} \frac{\varepsilon_{np}(E_{np}^{(+)})^2}{\varepsilon_{np}^2 - \omega_i^2}][\chi_- - \sum_{np} \frac{\varepsilon_{np}(E_{np}^{(-)})^2}{\varepsilon_{np}^2 - \omega_i^2}]$$

$$-\omega_i^2[\sum_{np}\frac{E_{np}^{(+)}E_{np}^{(-)}}{\varepsilon_{np}^2-\omega_i^2}]^2=0 \quad (9)$$

One of the characteristic quantities for the GT 1^+ states occurring in neighboring odd-odd nuclei is the GT transition matrix elements. The $0^+ \longrightarrow 1^+$ β^- and β^+ transition matrix elements are calculated as

$$M^i_{\beta^-}(0^+ \longrightarrow 1^+_i) =< 1^+_i,\mu|G^-_{1\mu}|0^+ >$$

$$=< 0|[Q_i(\mu),G^-_{1\mu}]|0 >$$

$$M^i_{\beta^-}(0^+ \longrightarrow 1^+_i) = -\sum_{np}(\psi^i_{np}b_{np}+\varphi^i_{np}\bar{b}_{np}), \quad (10)$$

$$M^i_{\beta^+}(0^+ \longrightarrow 1^+_i) =< 1^+_i,\mu|G^+_{1\mu}|0^+ >$$

$$=< 0|[Q_i(\mu),G^+_{1\mu}]|0 >$$

$$M^i_{\beta^+}(0^+ \longrightarrow 1^+_i) = \sum_{np}(\psi^i_{np}\bar{b}_{np}+\varphi^i_{np}b_{np}). \quad (11)$$

b_{np} and $\bar{b}_{np}$ are reduced matrix elements and they are given by

$$b_{np}=\frac{1}{\sqrt{3}}u_{j_n}v_{j_p} < j_n \parallel \sigma \parallel j_p >$$

$$\bar{b}_{np}=\frac{1}{\sqrt{3}}u_{j_p}v_{j_n} < j_n \parallel \sigma \parallel j_p > \quad (12)$$

where $v_{j_n}(u_{j_n})$ is the occupation (unoccupation) amplitude which is obtained in the BCS calculations. The $\beta^\pm$ reduced matrix elements are given by:

$$B^{(\pm)}_{GT}(\omega_i)=\sum_\mu |M^i_{\beta^\pm}(0^+ \longrightarrow 1^+_i|^2. \quad (13)$$

The $\beta^\pm$ transition strengths ($S^\pm$) defined as

$$S^\pm=\sum_i B^{(\pm)}_{GT}(\omega_i), \quad (14)$$

should fulfill the Ikeda Sum Rule (ISR)

$$ISR=S^{(-)}-S^{(+)}\cong 3(N-Z). \quad (15)$$

2.1.2 Odd-A Nuclei

In pn-QRPA, wave function of the i^{th} excited state in odd-A nuclei is given by

$$|\psi^j_{I_nK_n}\rangle=\Omega^{j^\dagger}_{I_nK_n}|0\rangle=[N^j_{I_n}\alpha^\dagger_{I_nK_n}$$

$$+\sum_{iI_pK_p}R^{I_nI_p}_{ij}(I_pK_p1K_n-K_p/I_nK_n)Q^\dagger_i\alpha^\dagger_{I_pK_p}]|0\rangle, \quad (16)$$

where I is the total angular momentum and K is the projection of I on the nuclear symmetry axis. It is assumed that wave functions for odd-A nuclei is formed by superposition of the one quasi-particle, and three quasi-particle (one quasi-particle + phonon) states. The mixing amplitudes $N_{I^j_n}$ and $R^{I_nI_p}_{ij}$ are fulfilled by the normalization condition

$$(N^j_{I_n})^2+\sum_{iI_p}(R^{I_nI_p}_{ij})^2=1. \quad (17)$$

The energies and wave functions of the odd-A nuclei are obtained from the pn-QRPA equation of motion:

$$[H,\Omega^{j^\dagger}_{I_nK_n}]|0\rangle=W^j_{I_nK_n}\Omega^{j^\dagger}_{I_nK_n}|0\rangle. \quad (18)$$

the dispersion equation for excitation energies $W^j_{I_nK_n}$, corresponding to states given in Eq. (16), is obtained as

$$W^j_{I_nK_n}-E_{I_nK_n}=$$

$$2\sum_{i,I_p,K_p}\frac{[X^{ph}_{GT}(d_{I_nI_p}M^+_i+\overline{d}_{I_nI_p}M^-_i)-X^{pp}_{GT}(b_{I_nI_p}F^+_i+\overline{b}_{I_nI_p}F^-_i)]^2}{W^j_{I_nK_n}-w_i-E_{I_pK_p}} \quad (19)$$

Where $E_{I_nK_n}$ and $E_{I_pK_p}$ are neutron and proton single quasi particle energies. The amplitude for three quasi-particle state state,$R^{I_nI_p}_{ij}$, is written in terms of the amplitude for one quasi-particle state, $N^j_{I_n}$, as follows:

$$R^{I_nI_p}_{ij}=$$

$$\frac{\sqrt{2}[X^{ph}_{GT}(d_{I_nI_p}M^+_i+\overline{d}_{I_nI_p}M^-_i)-X^{pp}_{GT}(b_{I_nI_p}F^+_i+\overline{b}_{I_nI_p}F^-_i)]}{W^j_{I_nK_n}-w_i-E_{I_pK_p}}N^j_{I_n} \quad (20)$$

where $N^j_{I_n}$ is calculated from Eq. (17). The corresponding expressions for the nuclei with odd-proton number are formulated by performing the transformation $I_nK_n \leftrightarrow I_pK_p$ in Eqs. (16)-(20). The GT transition matrix elements of odd-A nuclei is given by

$$M_{\beta^\pm}=\langle\psi^f_{I_1K_1}|\beta^\pm_\mu|\psi^i_{I_2K_2}\rangle. \quad (21)$$

The corresponding matrix elements of odd-A transitions are expressed for two different cases as follows:

(a) The case in which the number of pair does not change:

$$M_{\beta^-} = \langle \psi^f_{I_pK_p} | \beta^-_\mu | \psi^i_{I_nK_n} \rangle =$$

$$-[d_{I_nI_p} N^i_{I_n} N^f_{I_p} + \bar{d}_{I_nI_p} \sum_j R^{I_nI_p}_{ij} R^{I_nI_p}_{fj}$$

$$+N^i_{I_n} \sum_j R^{I_nI_p}_{fj} M^-_j + N^f_{I_p} \sum_j R^{I_nI_p}_{ij} M^+_j]. \quad (22)$$

$$M_{\beta^+} = \langle \psi^f_{I_nK_n} | \beta^+_\mu | \psi^i_{I_pK_p} \rangle =$$

$$-[d_{I_nI_p} N^i_{I_n} N^f_{I_p} + \bar{d}_{I_nI_p} \sum_j R^{I_nI_p}_{ij} R^{I_nI_p}_{fj}$$

$$+N^i_{I_p} \sum_j R^{I_nI_p}_{fj} M^+_j + N^f_{I_n} \sum_j R^{I_nI_p}_{ij} M^-_j. \quad (23)$$

(b) The case in which the number of pair changes:

$$M_{\beta^-} = \langle \psi^f_{I_nK_n} | \beta^-_\mu | \psi^i_{I_pK_p} \rangle$$

$$= -[\bar{d}_{I_nI_p} N^i_{I_p} N^f_{I_n} + d_{I_nI_p} \sum_j R^{I_nI_p}_{ij} R^{I_nI_p}_{fj}$$

$$+N^i_{I_p} \sum_j R^{I_nI_p}_{fj} M^-_j + N^f_{I_n} \sum_j R^{I_nI_p}_{ij} M^+_j]. \quad (24)$$

$$M_{\beta^+} = \langle \psi^f_{I_pK_p} | \beta^+_\mu | \psi^i_{I_nK_n} \rangle$$

$$= -[\bar{d}_{I_nI_p} N^i_{I_n} N^f_{I_p} + d_{I_nI_p} \sum_j R^{I_nI_p}_{ij} R^{I_nI_p}_{fj}$$

$$+N^i_{I_n} \sum_j R^{I_nI_p}_{fj} M^+_j + N^f_{I_p} \sum_j R^{I_nI_p}_{ij} M^-_j], \quad (25)$$

where $\mu = K_f - K_i . d_{np}$ and $\bar{d}_{np}$ are also reduced matrix elements and they are given by

$$d_{np} = \frac{1}{\sqrt{3}} u_{j_p} u_{j_n} < j_n \parallel \sigma \parallel j_p >$$

$$\bar{d}_{np} = \frac{1}{\sqrt{3}} v_{j_n} v_{j_p} < j_n \parallel \sigma \parallel j_p > \quad (26)$$

The reduced transition probability for the $I_iK_i \longrightarrow I_fK_f$ transitions in the laboratory frame is expressed by

$$B^{\pm}_{GT}(I_iK_i \rightarrow I_fK_f) =$$

$$\frac{g^2_A}{4\pi} (I_iK_i 1K_f - K_i/I_fK_f)^2 |M_{\beta^\pm}|^2, \quad (27)$$

The formalism used in PM is also used in Schematic Model (SM) with one major difference. The effective interaction term (h_0) is not added to the total Hamiltonian in the SM (for further details, see Refs. (35; 36; 43; 45; 46)).

2.2 The pn-QRPA Method

The Hamiltonian of the pn-QRPA model is given by

$$H^{QRPA} = H^{sp} + V^{pair} + V^{ph}_{GT} + V^{pp}_{GT}, \quad (28)$$

and it is diagonalized as outlined below. Single particle energies and wave functions are calculated in the Nilsson model which takes into account nuclear deformation (for our Model (C)). Pairing is treated in the BCS approximation. Details of these two steps can be seen from Ref. (41) and they are not reproduced here to save space.

In the pn-QRPA formalism, GT transitions are expressed in terms of phonon creation and one defines the QRPA phonons as

$$A^+_\omega(\mu) = \sum_{pn} (X^{pn}_\omega(\mu) a^+_p a^+_{\overline{n}} - Y^{pn}_\omega(\mu) a_n a_{\overline{p}}). \quad (29)$$

The sum in Eq. (29) runs over all proton-neutron pairs with $\mu = m_p - m_n = -1, 0, 1$, where $m_{p/n}$ denotes the third component of the angular momentum. The ground state of the theory is defined as the vacuum with respect to the QRPA phonons, $A_\omega(\mu)|QRPA\rangle = 0$. The forward and backward-going amplitudes X and Y are eigenfunctions of the RPA matrix equation

$$\begin{bmatrix} A & B \\ -B & -A \end{bmatrix} \begin{bmatrix} X \\ Y \end{bmatrix} = \omega \begin{bmatrix} X \\ Y \end{bmatrix}, \quad (30)$$

where ω are energy eigenvalues. Again we refer to (41) and references therein for solution of the RPA equation (30).

The proton - neutron residual interaction occurs through two channels: pp and ph channels. Both the interaction terms can be given a separable form. The ph force is given by

$$V^{ph}_{GT} = 2\chi \sum_\mu (-1)^\mu Y_\mu Y^+_{-\mu},$$

with

$$Y_\mu = \sum_{j_n j_p} \langle j_p m_p | t_- \sigma_\mu | j_n m_n \rangle c^+_{j_p} m_p c_{j_n m_n}, \quad (31)$$

whereas the pp interaction given by the separable force

$$V^{pp}_{GT} = 2\kappa \sum_\mu (-1)^\mu P_\mu P^+_{-\mu},$$

with

$$P^+_\mu = \sum_{j_n j_p} \langle j_n m_n | (t_- \sigma_\mu)^+ | j_p m_p \rangle$$

$$\times (-1)^{l_n + j_n - m_n} C^+_{j_p m_p} C^+_{j_n - m_n}, \quad (32)$$

is taken into account (in Models (B) and (C)). The interaction constants χ and κ in units of MeV are both taken to be positive. The different sings of V^{pp} and V^{ph} reflect a well-known feature of the nucleon-nucleon interaction: the ph force is repulsive while the pp force is attractive. For further details see Ref. (41). The reduced transition probabilities for GT transitions from the QRPA ground state to one-phonon states in the daughter nucleus are obtained as

$$B^\pm_{GT}(\omega) = |\langle \omega, \mu \| t_\pm \sigma_\mu \| QRPA \rangle|^2. \quad (33)$$

For odd-A nuclei, there exist two different types of transitions: (a) phonon transitions with the odd particle acting only as a spectator and (b) transitions of the odd particle itself. For case (b) phonon correlations are introduced to one-quasiparticle states in first-order perturbation. For further details, we refer to (41).

In order to improve the reliability of calculated results in pnQRPA (C) and SM (c) models, experimentally adopted value of the deformation parameter for ^{42,44,46,48,50}Ti, extracted by relating the measured energy of the first 2^+ excited state with the quadrupole deformation, was taken from Raman et al. (47). For all other cases, where measurement has not been so far done, the deformation of the nucleus was calculated using

$$\delta = \frac{125(Q_2)}{1.44(Z)(A)^{2/3}}, \quad (34)$$

where Z and A are the atomic and mass numbers, respectively and Q_2 is the electric quadrupole moment taken from Ref. (48). Q-values were taken from the recent mass compilation of Audi et al. (49).

3 GT$_\pm$ Strength Distributions

In a sense both β-decay and capture rates are very sensitive to the location of the GT$_+$ centroid. An (n,p) experiment on a nucleus (Z,A) shows the place where in $(Z-1,A)$ the GT$_+$ centroid corresponding to the ground state of (Z,A) resides. The β-decay and electron capture rates are exponentially sensitive to the location of GT$_+$ resonance while the total GT strength affect the stellar rates in a more or less linear fashion (50). Each excited state of (Z,A) has its own GT$_+$ centroid in $(Z-1,A)$ and all of these resonances must be included in the stellar rates. We do not have the ability to measure these resonances. Similar is the case in the β^- direction. Here, every excited state of (Z,A) also has its own GT$_-$ centroid in $(Z+1,A)$ and again all the contributions should be included in a reliable estimate of stellar β^--decay rates. Turning to theory, we see that the pioneer calculation done by Fuller and collaborators (51) (referred to as FFN throughout this text) had to revert to approximations in the form of Brink's hypothesis and "back resonances" to include all resonances in their calculation. Brink's hypothesis states that GT strength distribution on excited states is *identical* to that from ground state, shifted *only* by the excitation energy of the state. GT back resonances are the states reached by the strong GT transitions in the inverse process (electron capture) built on ground and excited states. Even the microscopic large-scale shell model calculations (52) had to use the Brink assumption to include all states and resonances. On the other hand, the pn-QRPA model is the only model that provides a microscopic way of calculating the GT$_\pm$ centroid and the total GT$_\pm$ strength for *all* parent excited states and it can lead to a fairly reliable estimate of the total stellar rates. The PM and SM have so far not been used to calculate excited state GT strength functions.

In this section, our calculation results for GT strength distribution function by using different models (pn-QRPA, PM and SM) are given. As discussed previously, we sub-divide the pn-QRPA and SM into three categories (A), (B) and (C). Model (A) is the most basic model in which only the interaction in ph channel is considered. Model (B) is to check the difference in calculations when one also incorporates pp force. Model (C) highlights the dependence of QRPA calculations on nuclear deformations. PM is classified only into two categories namely (A) and (B). The GT strength extracted from (p,n) spectra is about 40% lower than the Ikeda sum rule (53). Two possible mechanisms behind quenching of GT strength are pure nucleonic mechanism and Δ mechanism. For further details we refer to (54). El-Kateb and collaborators (4) employed a much

smaller quenching factor of 0.23 for ^{55}Mn, 0.31 for ^{56}Fe and ^{58}Ni for strength below 10 MeV excitation to compare shell model calculation with the measured data. Our calculated GT strengths are all quenched within the pn-QRPA formalism by universal factor of $f_q^2 = (0.6)^2$ which is used for fp shell nuclei (also employed in Ref. (22)). The re-normalized Ikeda sum rule in pn-QRPA is given by

$$ISR_{renorm} = S^{(-)} - S^{(+)} \cong 3f_q^2(N-Z). \quad (35)$$

Rather than presenting the detailed GT strength distributions for the twenty-one isotopes of titanium using the eight different models mentioned above, the key statistics of GT strength distribution (total strength, centroid and width) are shown in Tables 1 to 4. It is noted that the re-normalized Ikeda sum rule is fulfilled by pn-QRPA models (deviations are within a few percent and are attributed to non-nucleonic effects). The Ikeda Sum Rule in SM and PM models is given by Eq. 13. Total strength calculations are performed up to 20 MeV in pn-QRPA whereas in PM and SM models they are calculated up to 40 MeV.

Table 1 displays the calculated total GT strengths, centroids and widths for isotopes of titanium ($^{40-44}$Ti) in both β-decay and electron capture directions. Results are shown for all eight models (which are also explained in the footnote of Table 1). Centroids and widths are given in units of MeV and B(GT) strengths are given in units such that B(GT) = 3 for neutron decay.

As seen from Table 1, the calculated values for ^{40}Ti show that PM and SM models give much bigger values for total GT strength in electron capture direction. The centroids are also placed at higher excitation energies in daughter nuclei for the PM and SM models. These two models also generally calculate bigger widths than the corresponding results of pn-QRPA model. The effect of the inclusion of the pp interaction in pinning down the centroid values is more pronounced in PM model (they approximately decrease to half their original values). However, pp force does not show any similar change in other calculated quantities by remaining two models. The pn-QRPA model calculates the lowest centroids and widths.

For the case of odd-A nucleus ^{41}Ti, one notes that for electron capture direction, the pn-QRPA (C) calculates bigger total strength as compared to pn-QRPA (A) and (B). In the β-decay direction, the three pn-QRPA models show close results. The SM (C) and PM (B) models bring substantial improvement over SM (A), SM (B) and PM (B) models leading to much lower values of centroids and widths in β-decay direction and bigger total GT strength values. SM (C) calculates lowest centroid and biggest strengths for ^{41}Ti.

The B(GT) values, centroids and widths for ^{42}Ti calculated by the pn-QRPA model decrease when the pp interaction for spherical case is taken into account (compare versions (A) and (B)), albeit not much. Deformation substantially changes the pn-QRPA results for total strength and centroid. PM (B) brings down the calculated centroid values roughly by a factor of three and at the same time increases the total strength and width values in both directions. The pp force in PM method pins down the centroid values but results in no significant changes in the calculated values of total strength and width. The role of pp force in SM model for spherical case increases the total strengths, centroids and widths. However, when the pp force is considered together with deformation, the centroids and widths are roughly halved and at the same time there is an increase in total strength values. The pp force in all models assists in shifting the centroid to lower excitation energies in daughter.

No appreciable difference is seen among the three pn-QRPA models for the case of ^{43}Ti specially in the β-decay direction. On the other hand, SM (C) not only substantially changes the results of SM (A) and SM (B) but also calculates lower widths and centroids as compared to pn-QRPA (C). Moreover, SM (C) is also able to calculate bigger total strength, especially in β-decay direction. PM (A) and PM (B) give smaller B(GT) values than pn-QRPA and SM models. The effect of the incorporated deformation is significant in the case of SM.

The calculated results for ^{44}Ti have been presented as a last entry in Table 1. The biggest and lowest values for total strengths have been obtained by the SM (C) and PM (A) models, respectively. PM model values calculate very small GT strength. All three models do not exhibit any substantial change in calculated quantities in the given versions. Deformation tends to increase total strength, centroid and width values in SM model. SM and pn-QRPA models have around three times larger B(GT) values than the PM models. For the case of centroids and widths, the results of PM models are approximately three times bigger than the corresponding ones in SM and pn-QRPA models.

The key statistics for calculated GT transitions in $^{45-50}$Ti are presented in Table 2. For ^{45,47,49}Ti there is no much appreciable change in the results of all quantities calculated by pn-QRPA and PM models for β^- and β^+ decay. For the case of ^{45}Ti, PM (A), PM (B) and SM (B) calculate small total strength in both directions. The effect of the pp force does not change significantly the results in PM model. Deformation provides a drastic decrease in widths of the calculated GT distributions

for SM model. The centroid values in PM model are appreciably low. On the other hand, the calculated width values in PM models for β^- and β^+ decays are bigger than the corresponding results in SM and pn-QRPA models. For ^{47}Ti, SM (C) makes a significant change in the centroid, width and total strength values. The effect of the incorporated deformation in the three models is most pronounced in SM and least in pn-QRPA. For ^{49}Ti, results are similar as in the case of ^{45,47}Ti. When deformation is taken into account the B(GT) values for β-decay in pn-QRPA and SM models increase by a factor of 2-3. PM models gives a very small total strength for β^+ decay. For the case of even-even isotopes ($^{46-50}$Ti), it is noted that no pronounced difference occurs among the results of pn-QRPA (A) and pn-QRPA (B) versions. One notes that pn-QRPA (B) version gives lower B(GT) and width values for both β^+ and β^- decay in ^{46,48}Ti. Vanishing total strength in β^+ direction is calculated for ^{48}Ti in PM models. In ^{50}Ti isotope, SM (C) model gives the highest centroid and width values amongst all other models.

In Table 3, the calculated total GT strengths, centroids and widths for $^{51-56}$Ti are shown for the three models. For ^{51,53,55}Ti, SM (C) calculates biggest total strength along β-decay direction. For the odd-A cases, SM (C) calculates the biggest total strength. The SM models tend to calculate largest centroid values along β-decay direction. The pn-QRPA models calculate the lowest centroid in β-decay direction for all Ti isotopes in Table 3.

Table 4 finally displays the calculated total strengths, widths and centroids for $^{57-60}$Ti. Isotopes of titanium gets progressively neutron-rich as one proceeds from Table 1 to Table 4. In Table 4, pn-QRPA (C) model calculates low centroids and reasonable GT strengths (satisfying renormalized Ikeda sum rule Eq. 29). PM model places centroids for β^--decay centroids in ^{58,60}Ti at much lower energies than the SM model. It can be seen that the total strength values in PM (A) and PM (B) models are very closer to the corresponding ones in SM (A) and SM (B) for ^{58,60}Ti. In ^{57,59}Ti, the calculated GT strength values increases substantially in SM (C) in accordance with the Ikeda sum rule.

Tables 1 to 4 show that the pn-QRPA models follow systematic trend in the calculation of GT strength function for both even-even and odd-A nuclei. The values of pn-QRPA calculated total strength decreases (increases) systematically, separately for even-even and odd-A nuclei, along the electron capture (β-decay) direction. This trend is valid only for even-even nuclei in PM and SM models. The pn-QRPA (C) is the best model for the calculation of GT strength distribution amongst all eight models presented in this work for even-even and odd-A nuclei. The pn-QRPA (C) model calculates reasonable total strength in both directions for all cases (see comparison with measured data below). Moreover, the model calculates lower centroid energies in daughter which translates into bigger weak interaction rates and can bear consequences for astrophysical applications. Further, it is only the pn-QRPA (C) model that fulfills the re-normalized Ikeda sum rule Eqt. (35). Only in the case of ^{55}Ti is the re-normalized sum rule satisfied to only 94%. The pn-QRPA (A) is not able to satisfy the sum rule for few odd-A cases whereas version (B) fails for few mixed cases. However, PM (B) model also shows good results of GT strength distributions for even-even nuclei. The PM (B) and SM (C) tend to fulfill the Ikeda sum rule Eqt. (15) for even-even nuclei. The PM (B) and SM (C) are the better model in its genre and shows overall better results in their class. The results support the argument that the QRPA models perform best when performed both in *pp* and *ph* channels, taking nuclear deformation into consideration.

So far we have only shown the mutual comparison of the calculated total GT strength distributions amongst the eight theoretical models. It would be interesting to see the comparison of the results for these models with the measured data where available. For this reason, we searched the literature and were able to find at least five cases of reported measured GT strength distributions of titanium isotopes (^{40,41,46,47,48}Ti). Next, we compare the measured data with the the results of three preferred models, namely pn-QRPA (C), SM (C) and PM (B). Moreover, we also compare our results for these cases with other theoretical calculations.

Fig. 1 shows the GT$_+$ strength distribution for ^{40}Ti. Liu and collaborators (38) studied the β decay of ^{40}Ti and ^{41}Ti and its subsequent implication for detection of solar neutrinos. Trinder et al. also made a study of the β-decay measurement of ^{40}Ti (55) at GANIL using the LISE3 spectrometer. For details of experiment, we refer to (55). The results of these two β-decay experiments are shown in top two panels of Fig. 1. In the top panel, Exp. 1 shows the measured data of Ref. (55) while Exp. 2 corresponds to that of Ref. (38). The third, fourth and fifth panels show our calculated results of pn-QRPA (C), SM (C) and PM (B) models, respectively. We also show the (0+2)$\hbar\omega$ shell model calculation of GT$_+$ strength distribution for ^{40}Ti in bottom panel performed by Ormand and collaborators (56). In order to bring their calculated GT strength in compliance with the measured GT data, the authors re-normalized the free nucleon GT operator by the factor 0.775 (56). The horizontal axis in Fig. 1 shows the energy scale in daughter ^{40}Sc in units of MeV. It can

be seen from Fig. 1 that the pn-QRPA (C) model reproduces well the low-lying measured GT strengths of Refs. (38; 55) and also predicts some GT transitions above 8 MeV in daughter which are not reported by measurements. Shell Model calculation (56) is in good agreement with the measured data. The pn-QRPA (C) calculated total strength, up to 15 MeV in daughter, is 6.00 and is in very good agreement with the measured strength of 5.86 (5.87) by Ref. (38) (Ref. (55)). Shell Model calculated a total strength of 5.62. The SM (C) and PM (B) models give a total strength value of 7.62 and 10.80, up to 15 MeV, and they are considerably bigger than the experimental values. The shell model data is not well fragmented as compared to pn-QRPA (C) data. This is possibly due to the neglect of higher-order correlations in the shell model. The pn-QRPA (C) model placed the GT centroid at 3.91 MeV in daughter and it is also in very good agreement with the measured data of 3.87 MeV by Ref. (38) and 3.78 MeV by Ref. (55). Shell model placed the centroid at 4.67 MeV whereas the PM(B) and SM (C) models placed the centroid at a too high excitation energy of 11.47 MeV and 12.17 MeV, respectively.

Honkanen et al. (57) performed an improved high-resolution study of the β-decay of ^{41}Ti produced in the ^{40}Ca(^{3}He,2n) reaction at 40 MeV at the IGISOL facility (57). In addition, the authors also performed a shell model calculation of the GT strength distribution of ^{41}Ti in the *sdfp* space. For details of the experiment and theoretical shell model calculation, we refer to (57). We show the measured data by Honkanen and collaborators (57) as Exp. 1 in the top panel of Fig. 2. The measured GT strength distribution of ^{41}Ti by Liu et al. (38) is shown in second panel as Exp. 2. The next three panels show our calculated results for pn-QRPA (C), SM (C) and PM (B) models, respectively. In the bottom panel, we show the shell model calculation of Ref. (57). The measured data is well fragmented up to 8 MeV in daughter. The theoretical models calculate a well fragmented data, akin to measured data. All theoretical models do calculate high-lying GT transitions not reported by experiments. The Shell Model data calculates much bigger total strength of 10.92 which is to be compared with measured strength of 4.83 by Liu et al. and 4.34 by Honkanen and collaborators. The pn-QRPA (C) model calculates a total strength of 4.89 in excellent agreement with the measured value of 4.83 (38). The total strength calculated by the SM (C) is 4.36 in excellent agreement with the measured value of 4.34 (57) whereas the PM (B) model finds a total strength of 7.76. The centroid in the SM (C) model is placed at too high excitation energy of 8.13 MeV in ^{41}Sc. The pn-QRPA (C) calculated the centroid value of 8.96 MeV which can be compared with the shell model results of 7.86 MeV . In comparison, the centroids of measured data by Refs. (57) and (38) are at 5.27 MeV and 5.67 MeV, respectively. The PM (B) model gives a centroid value of 8.61 MeV. It is to be noted that whereas the measured data is available only up to an excitation energy of 8 MeV, the theoretical data are given up to an excitation energy of 15 MeV in daughter. If one cuts the theoretical data also till 8 MeV then the calculated centroids can come in reasonable agreement with the measured centroids. Fig. 2 shows that a quenching of GT strength calculated by shell model is in order. Experimentalists are urged to search for high-lying GT transitions (up to 15 MeV) in ^{41}Sc.

For the case of ^{46}Ti, there are quite a few theoretical GT calculations available in the β-decay direction. The results are shown in Fig. 3 which comprises of eight panels. The measured data was taken from the recent β-decay measurement of ^{46}Ti by Adachi and collaborators (58) and it is shown in the top panel of Fig. 3. The authors performed a high-resolution (^{3}He,t) experiment on ^{46}Ti at 0^{0} and at an intermediate incident energy of 140 MeV/nucleon for the study of precise measurement of GT transitions in ^{46}V. A very good energy resolution of $\Delta E \leq 50$ keV was realized in the experiment. For further details of the experiment, Ref. (58) can be seen. Besides our pn-QRPA (C), SM (C) and PM (B) models (shown in second, third and fourth panel, respectively), we also show the results of GT strength distributions from four other theoretical calculations. The large scale shell model (LSSM) calculation of Petermann et al. (59) is shown in the fifth panel. Petermann and collaborators used the KB3G interaction (60) and employed Lanczos method with 100 iterations ensuring convergence in their calculation for 1-2 MeV excitation energies. The sixth panel shows the quasideutron (QD) model calculation with a deformed core (i.e. rotor + quasideutron model) performed by Lisetskiy et al (61). The last two panels show shell model calculations using KB3G (60) and GXPF1 (62) interactions, respectively. All shell model data as well as the QD model used a quenching factor of $(0.74)^2$ in their calculations. It can be seen from Fig. 3 that the pn-QRPA (C) data is well fragmented and it is in good agreement with the β-decay measurement performed by Adachi et al. The pn-QRPA (C) model also calculates its strongest GT transition around 3 MeV akin to measured data. The SM (C) model calculates the fragmented GT strength distribution and high-lying transitions in the range of 6-12 MeV. The largest GT strength which is 4-8 times larger than other calculations and experimental result is obtained by PM (B) model. In this model, only one GT peak is seen around 9 MeV. The shell model results

do not produce enough fragmentation of GT strength, specially at low excitation energies (between 1 and 3 MeV). The QD model calculates only four transitions. In QD model, the low-lying states in ^{46}V are described by an angular-momentum-coupled proton-neutron pair (quasideutron) made of the valence odd proton and neutron occupying Nilsson orbits coupled to the rotating ^{44}Ti core. Table 5 presents the total GT strength as well as the calculated centroid for all GT distribution functions shown in Fig. 3. It can be seen from Table 5 that the QD model best reproduces the measured total GT strength up to 5.4 MeV in ^{46}V. Once again it is to be noted that LSSM, pn-QRPA (C), PM (B) and SM (C) have a high cutoff in daughter excitation energy and reducing this cutoff can lead to much better comparison with measured data. At the same time, experimentalists can be directed to perform their measurement up to around 15 MeV in daughter to look for more high-lying GT strength in ^{46}V.

A high resolution (^{3}He,t) experiment for ^{47}Ti was performed at the Research Center for Nuclear Physics, Japan at an intermediate incident energy of 140 MeV/nucleon and a very fine energy resolution of 20 keV. The measurement was reported recently (63) up to an excitation energy of 12.5 MeV in ^{47}V. The authors were suggestive that high-lying GT strength beyond 12.5 MeV might also exist well . The results of the measurement are shown in the top panel of Fig. 4. Once again we depict the calculated results of pn-QRPA (C), SM (C) and PM (B) in the second, third and fourth panel of Fig. 4, respectively. The bottom panel finally shows the shell model calculation using the GXPF1 interaction (62) including a quenching factor of $(0.74)^2$. The shell model and experimental results are generally in agreement. However, above 10 MeV, the shell model cumulative sum is larger than the experimental one. The pn-QRPA (C) data is also fragmented like the shell model and experimental data and it is in excellent agreement with the measured data. The SM (C) and PM (B) do not perform well for this odd-A isotope of titanium. The PM (B) calculates a peak value of 0.16 at a relative low excitation energy of 0.2 MeV whereas the SM (C) calculates the biggest transition of 1.04 magnitude at 11.6 MeV. The pn-QRPA (C) calculated a total strength of 3.58 in complete agreement with the measured value of 3.60. The corresponding value calculated within the shell model is 2.76. The SM (C) calculates yet smaller value of total strength of 2.47 whereas the PM (B) bags a paltry sum of 0.36. Regarding centroid placement, one notes that pn-QRPA (C) calculates the centroid at 7.62 MeV which is again in excellent agreement with the measured centroid of 7.5 MeV. LSSM fixes the centroid at 7.59 MeV. The SM (C) places the centroid at a higher value of 9.48 MeV and PM (B) places it at 4.45 MeV.

We finally present the GT strength distributions of ^{48}Ti (in the electron capture direction) in Fig. 5. Alford and collaborators (64) studied the ^{48}Ti(n,p) reaction at an energy of 200 MeV and they were able to obtain GT strength distribution of ^{48}Ti up to a comparatively much higher energy value of around 12 MeV in daughter nucleus, ^{48}Sc. Further details of the performed experiment can be seen from Ref. (64). The top panel of Fig. 5 shows the measured GT distribution obtained from the (n,p) reaction experiment. This is followed by our model calculations of pn-QRPA (C), SM (C) and PM (B). The bottom panel presents the shell model calculation by Brown (65) in a model space $(f_{7/2})^{8-n}(f_{5/2}p_{3/2}p_{1/2})^n$ with n = 0, 1, and 2. The shell model data has been quenched by a factor 0.6. It can be seen from Fig. 5 that the measured GT strength is well fragmented and extend to high excitation energies in ^{48}Sc. The pn-QRPA (C) calculation is also well fragmented. The first measured peak at 2.52 MeV is well reproduced by the pn-QRPA (C) model but it also calculates a strong peak of 0.6 at 2.64 MeV in ^{48}Sc. The SM (C) data is also fragmented but is off much lower strength. The shell model calculates the strongest peak of 0.6 at 6.44 MeV. The total measured GT strength of 1.44 is to be compared with the theoretical values of 1.78, 0.90, 0.26 and 1.08 by pn-QRPA (C), SM (C), PM (B) and shell model, respectively. The centroid of the measured GT distribution resides at 7.31 MeV in daughter. The pn-QRPA (C) model calculates a much lower centroid at 4.12 MeV. The SM (C) locates the centroid at 5.72 MeV whereas the shell model places it at 6.19 MeV in daughter ^{48}Sc. The highest centroid value has been obtained by PM (B) model which is 8.47 MeV. This value is higher than the measured data although the corresponding values for other theoretical calculations are lower than the experimental results. The closest match with the measured centroid value for the case of ^{48}Ti is provided by shell model calculation.

4 Summary and conclusions

Fermi and Gamow-Teller transitions are required for an accurate calculation of β-decay and electron capture rates in terrestrial and stellar environments. Reliable estimates of β-decay half-lives (including many neutron-rich nuclei) are in high demand in various nuclear physics (e.g. for the experimental exploration of the nuclear landscape at existing and future radioactive ion-beam facilities) and astrophysical problems (e.g. for a better understanding of the supernova explosion

mechanism and heavy element nucleosynthesis). It is the GT transitions which are fragmented and are very challenging to calculate. The GT transitions assume a nuclear model for its calculation whereas calculation of Fermi transitions is straight forward (these are concentrated in a single state known as isobaric analogue state). The Gamow-Teller strength distribution for isotopes of titanium, $^{40-60}$Ti, were calculated and analyzed by using three microscopic models (namely the pn-QRPA, Pyatov Method and Schematic Method). The pn-QRPA and Schematic model were further subdivided into three classes in order to highlight the role of particle-particle (pp) force and deformation of the nucleus in the GT strength calculation within the models. In Pyatov Method, only the effect of the pp force was studied. The calculated GT strength functions were compared with the corresponding experimental and other theoretical model calculations wherever available. The isotopes of titanium chosen for this project also included neutron-rich cases and have astrophysical significance.

Our calculations strongly suggest that models with *pp* force and deformation of nucleus incorporated give better results for GT strength distribution functions.

The calculations show that the inclusion of pp interaction and deformation in pn-QRPA model tends to bring down the centroid values. In PM and SM models, the pp force has a rather unpredictable effect on centroid placement. Further, in general, for the case of SM and PM models, the pp force does not show any sharp change in width and GT strength calculations (see Tables 1 to 4). Centroid placement in SM is generally at higher excitation energies as compared to the PM even though the same effective interaction constant values (χ_{ph} and χ_{pp}) are used in both models. Lower centroids are attributed to the inclusion of h_0 in PM models.

The calculated GT strength distribution functions were also compared with measured GT distributions where available. Comparison with other theoretical calculations were also sought in such cases. The pn-QRPA (C) is best able to reproduce the measured strength and centroid of ^{40}Ti. The shell model calculated total strength is also in good agreement with the measured strength of ^{40}Ti. For the case of ^{41}Ti, both the pn-QRPA (C) and SM (C) models were able to reproduce the measured total strength. All theoretical models calculated high-lying GT transitions for ^{41}Ti not reported by measurements. The QD model best reproduces the measured GT strength function in ^{46}V. For ^{47}Ti, the pn-QRPA (C) best reproduces the measured total strength and centroid placement (shell model calculated centroid is also in agreement with measured data). For ^{48}Ti, shell model is successful in reproducing the measured GT strength function.

The pn-QRPA (C) model satisfied the re-normalized Ikeda sum rule to within a few percent and calculated much bigger GT strengths and lower centroids as compared to other QRPA models. The model also followed a systematic trend in calculation of GT strength for even-even and odd-A titanium isotopes. This trend is valid only for even-even nuclei in PM and SM models. The pn-QRPA (C) model also performed reasonably well in comparison to measured GT strength distributions. SM (C) model also displayed encouraging results.

One expects significant progress in our understanding of supernova explosions and heavy element nucleosynthesis to come from next-generation radioactive ion-beam facilities (e.g. FAIR (Germany), FRIB (USA) and FRIB (Japan)) when we would have access to measured GT strength distribution of many more nuclei (including unstable isotopes). Nonetheless, for astrophysical applications, one needs microscopic and reliable calculation of GT strength distributions for hundreds of iron-regime nuclei. We are in a process of calculating GT strength functions for other key *fp*-shell nuclei (including many neutron-rich unstable nuclei) in a microscopic fashion and hope to report our findings in near future.

Acknowledgements S. Cakmak and T. Babacan would like to acknowledge the support of research grant provided by BAP Project with number 2013-004. S. Cakmak would also like to acknowledge the kind hospitality provided by the GIK Institute of Engineering Sciences and Technology, Pakistan, where major portion of this project was completed and manuscript written.

References

F. Osterfeld.: Nuclear-Spin And Isospin Excitations. Rev. Mod. Phys. **64**, 491 (1992).

Ikeda K., Fujii S., Fujita J. I.: The (p,n) reactions and beta decays. Phys. Lett. **3**, 271 (1963).

Anderson B. D.,Tamimi N., Baldwin A. R., Eleasir M., Madey R., Manley D. M., Mostajabodda'vati M., Watson J. W., Zhang W. M.and Foster C. C.: Gamow-Teller strength in (p, n) reaction at 136 MeV on ^{20}Ne,^{24}Mg and ^{28}Si. Phys. Rev. C **43** 1 (1991).

El-Kateb S., Alford W. P., Abegg R., Azuma R. E., Brown B. A., Celler A., Frekers D., Häusser O., Helmer R., Henderson R. S., Hicks K.H., Jeppesen R., King J.D., Raywood K., Shute G.G., Spicer B.M., Trudel A., Vetterli M. and Yen S.: Spin-isospin strength distributions for fp shell nuclei: Results for the ^{55}Mn(n,p), ^{56}Fe(n,p), and ^{58}Ni(n,p) reactions at 198 MeV. Phys. Rev. C **49** 3128 (1994).

Fujita Y., Akimune H., Daito I., Fujimura H., Fujiwara M., Harakeh M. N., Inomata T., Jänecke J., Katori K., Tamii A., Tanaka M., Ueno H., and Yosoi M.:Mirror-symmetry structure of $A = 27$, $T = 1/2$ nuclei studied through strong, weak, and electromagnetic interactions. Phys. Rev. C **59**, 90 (1999)

Cole A.L., Akimune H., Austin Sam M., Bazin D., Berg A. M. van den, Berg G.P.A., Brown J., Daito I., Fujita Y., Fujiwara M., Gupta S., Hara K., Harakeh M.N., Janecte J., Kawabata T., Nakamura T., Roberts D.A., Sherrill B.M., Steiner M., Ueno H., and Zegers R.G.T.:Measurement of the Gamow-Teller strength distribution in ^{58}Co via the ^{58}Ni(t,^{3}He) reaction at 115 MeV/nucleon. Phys. Rev. C **74**, 034333 (2006)

Bäumer C., Berg A.M. van den, Davids B., Frekers D., Frenne S. De, Grewe E.-W., Haefner P.,Harakeh M.N., Hofmann F., Hollstein S., Hunyadi M., Huu M. A. de, Jacobs E., Junk B.C., Korff A., Langanke K., Martínez-Pinedo G., Negret A., Neumann-Cosel P. von, Rakers S., Richter A., and Wörtche H. J.: Determination of the Gamow-Teller strength distribution from the odd-odd nucleus ^{50}V measured through $^(50)$V(d,^{2}He)^{50}Ti and astrophysical implications. Phys. Rev. C **71**, 024603 (2005).

Bertulania C.A., Lotti P.:Fermi and Gamow-Teller strength in charge exchange with radioactive beams. Phys. Lett. B **402** 237-242 (1997)

Martínez-Pinedo G., Langanke K., Dean D. J.: Competition of electron capture and beta-decay rates in supernova collapse. Astrophys. J. Suppl. Ser.**126**, 493 (2000).

Caurier E., Martínez-Pinedo G., Nowacki F., Poves A., Zuker A. P.: The shell model as a unified view of nuclear structure. Rev. Mod. Phys. **77**, 427 (2005).

Halbleib J. A. and Sorensen R. A.: Gamow-Teller beta decay in heavy spherical nuclei and the unlike particle-hole rpa. Nucl. Phys. A**98**, 542 (1967).

Krumlinde J. and Möller P.: Calculation of Gamow-Teller β-strength functions in the rubidium region in the rpa approximation with Nilsson-model wave functions. Nucl. Phys. A**417**, 419 (1984).

Muto K., Bender E., Oda T. and Klapdor-Kleingrothaus H. V.: Proton-neutron quasiparticle RPA with separable Gamow-Teller forces. Z. Phys. A **341**, 407 (1992).

Nabi J.-Un and Klapdor-Kleingrothaus H. V.: Weak Interaction Rates of sd-Shell Nuclei in Stellar Environments Calculated in the Proton-Neutron Quasiparticle Random-Phase Approximation. At. Data Nucl. Data Tables **71**, 149 (1999).

Nabi J.-Un, Klapdor-Kleingrothaus H. V.: Microscopic calculations of stellar weak interaction rates and energy losses for fp- and fpg-shell nuclei. At. Data Nucl. Data Tables **88**, 237 (2004).

Nabi J.-Un and Klapdor-Kleingrothaus H. V.: Microscopic calculations of weak interaction rates of nuclei in stellar environment for A = 18 to 100. Eur. Phys. J. A **5**, 337 (1999).

Nabi J.-Un and Rahman M.-Ur.: Gamow-Teller strength distributions and electron capture rates for ^{55}Co and ^{56}Ni. Phys. Lett. **B612**, 190 (2005).

Nabi J.-Un, Sajjad M., Rahman M.-Ur: Electron capture rates on titanium isotopes in stellar matter. Acta Physica Polonica B **38**, 3203 (2007).

Nabi J.-Un and Sajjad M.: Neutrino energy loss rates and positron capture rates on ^{55}Co for presupernova and supernova physics. Phys. Rev. C**77**, 055802 (2008).

Nabi J.-Un.: Weak-interaction-mediated rates on iron isotopes for presupernova evolution of massive stars. Eur. Phys. J. A **40**, 223 (2009).

Nabi J.-Un.: Expanded calculation of neutrino cooling rates due to ^{56}Ni in stellar matter. Phys. Scr.**81**, 025901 (2010).

Nabi J.-Un.: Ground and excited states Gamow-Teller strength distributions of iron isotopes and associated capture rates for core-collapse simulations. Astrophys Space Sci. **331**, 537 (2011).

Nabi J.-Un.: Nickel isotopes in stellar matter. Eur. Phys. J. A **48**, 84 (2012).

Nabi J.-Un and Johnson C. W.: Comparison of Gamow-Teller strengths in the random phase approximation. J. Phys. G **40**, 065202 (2013).

Pyatov N. I. and Salamov D. I.: Conservation laws and collective excitations in nuclei. Nucleonica **22**, 127 (1977).

PM Dirac: Lecture in Quantum Mechanics, Yeshiva University Press, New York 1964

Civitarese O. and Licciardo M. C: Symmetry restoring treatment of the pairing Hamiltonian in quasiparticle representation. Phys. Rev. C **38**, 967 (1988).

Civitarese O. and Licciardo M. C: Comparison between effective Hamiltonians in symmetry restoring theories. Phys.Rev. C **41**, 1778 (1990).

Civitarese O., Faessler A. and Licciardo M. C.: Symmetry breaking of the Galilean invariance in superfluid nuclei and its connection with quadropole pairing interactions. Nucl. Phys. A **542**, 221 (1992).

Sakamoto K. T.: Microscopic analysis of nuclear collective motions in terms of the boson expansion theory: Numerical calculations. Nucl. Phys. A **528**, 73 (1991).

Civitarese O., Hess P. D., Hirsch J. G. and Reboiro M.: Spontaneous and dynamical breaking of mean field symmetries in the proton neutron quasi particle random phase approximation., Phys. Rev. C **59**, 194 (1998).

Magierski P. and Wyss R.: Self consistent effective interactions and symmetry restoration. Phys. Lett. B **468**, 54 (2000).

Kulliev A. A., Akkaya R., Ilhan M., Guliev E., Salamov C. and Selvi S.: Rotational invariant model of the states with $K^\pi = 1^+$ and their contribution to the scissors mode. Int. J. Modern Phys. E **9**, 249 (2000).

Babacan T., Salamov D. I. and Kucukbursa A.: The effect of the pairing interaction on the energies of isobar resonanse in $^{112-124}$Sb and isospin admixture in $^{100-124}$Sn isotopes. J. Phys. G **30**, 759 (2004).

Babacan T., Salamov D. I. and Kucukbursa A.: Gamow-Teller 1^+ states in ^{208}Bi. Phys. Rev. C **71**, 037303 (2005).

Babacan T., Salamov D. I. and Kucukbursa A.: The investigation of the log(ft) values for the allowed Gamow-Teller transitions of some deformed nuclei. Math. Comp. Application **10**, 359 (2005).

Sarkar S. and Pramana J.: Relevance of thermally populated first excited state of ^{44}Ti to the abundance problem of Cassiopiea A: A model study. Phys **53**, 469 (1999).

Liu W., Hellström M., Collatz R., Benlliure J., Chulkov L., Cortina Gil D., Farget F., Grawe H., Hu Z., Iwasa N., Pfützner M., Piechaczek A., Raabe R., Reusen I., Roeckl E., Vancraeynest G. and Wöhr A. : β decay of ^{40}Ti and ^{41}Ti and implication for solar-neutrino detection. Phys. Rev. C **58**, 2677 (1998).

Aufderheide M. B., Fushiki I., Woosley S. E., Stanford E. and Hartmann D. H.: Search for important weak interaction nuclei in presupernova evolution. Astrophys. J. Suppl. Ser.**91**, 389 (1994).

Heger A., Woosley S. E., Martínez-Pinedo G. and Langanke K.: Presupernova evolution with improved rates for weak interactions. Astrophys. J. **560**, 307 (2001).

Hirsch M., Staudt A., Muto K. and Klapdor-Kleingrothaus H. V.: Microscopic predictions of β^+/EC-decay half-lives. At. Data Nucl. Data Tables **53**, 165 (1993).

Stetcu I. and Johnson C. W.: Gamow-Teller transitions and deformation in the proton-neutron random phase approximation. Phys. Rev. C**69**, 024311 (2004).

Cakmak N., Unlu S. and Selam C.:Gamow-Teller 1^+ states in $^1 12 - 124$Sb isotopes, Indian Academy of Sciences, **75**, 649-663 (2010)

Salamov D.I. et. al.: Proceedings of 5th Conference on Nuclear and Particle Physics (NUPPAC 05) (Cairo, August 2006), p. 361

Selam C., Babacan T., Bircan H., Aygor H.A., Kucukbursa A. and , Maras I. :The investigation of the Log(ft) Values for the Allowed Gamow-Teller Transitions of Some Deformed Nuclei, Mathematical Computational Applications, **9**, No. 1, pp. 79-90 (2004)

Salamov D.I.,Kucukbursa A., Maras I.,Aygor H.A., Babacan T. and Bircan H.: Calculation of the Log(ft) Values for the Allowed Gamow-Teller Transitions in Deformed Nuclei Using the Basis of Woods-Saxon Wave Functions, Acta Physica Slovaca, **53**,pp.307-319 (2003)

Raman S., Malarkey C.H., Milner W.T., Nestor, Jr. C.W., Stelson P.H.: Transition Probability, B(E2)↑, from the Ground to the First-Excited 2^+ State of Even-Even Nuclides. At. Data Nucl. Data Tables **36**, 1 (1987)

Möller P., Nix J.R.: Atomic Masses and Nuclear Ground-State Deformations Calculated with a New Macroscopic-Microscopic Model. At. Data Nucl. Data Tables **26**, 165 (1981)

Audi G., Wapstra A.H., Thibault C.: The AME2003 Atomic Mass Evaluation (II). Tables, Graphs and References. Nucl. Phys. A**729**, 337 (2003)

Aufderheide M. B., Bloom S. D., Mathews G. J. and Resler D. A.: Importance of (n,p) reactions for stellar beta decay rates. Phys. Rev. C **53**, 3139 (1996).

Fuller G. M., Fowler W. A., Newman M. J.: Stellar weak-interaction rates for sd-shell nuclei. I. nuclear matrix element systematics with application to ^{26}Al and selected nuclei of importance to the supernova problem. Astrophys. J. Suppl. Ser.**42**, 447 (1980); Stellar weak interaction rates for intermediate mass nuclei. II. A = 21 to A = 60. Astrophys. J. **252**, 715 (1982); Stellar weak interaction rates for intermediate mass nuclei. III. Rate tables for the free nucleons and nuclei with A = 21 to A = 60. Astrophys. J. Suppl. Ser. **48**, 279 (1982); Stellar weak interaction rates for intermediate mass nuclei. IV. Interpolation procedures for rapidly varying lepton capture rates using effective log (ft)- values. Astrophys. J. **293**, 1 (1985).

Langanke K. and Martínez-Pinedo G.: Shell-Model calculations of stellar weak interaction rates: II. Weak rates for nuclei in the mass range A = 45-65 in supernovae environments. Nucl. Phys. A**673**, 481, (2000).

Gaarde C. et al. Proc. Int. Symp. Nuclear Spectroscopy and Nuclear Interactions, Osaka, eds. Ejiri E and Fukuda T (singapore: World Scientific), 359 (1984).

Grotz K, and Klapdor H. V.: The Weak Interaction in Nuclear, Particle and Astophysics. IOP Publishing Limited 1990.

Trinder W., Anne R., Lewitowicz M., Saint-Laurent M. G., Donzaud C., Guillemaud-Mueller D., Leenhardt S., Mueller A. C., Pougheon F., Sorlin O., Bhattacharya M., García A., Kalokamis N. I., Adelberger E. G. and Swanson H. E.: ^{40}Ti β decay and the neutrino capture cross section of ^{40}Ar. Phys. Lett. B **415**, 211 (1997).

Ormand W. E., Pizzochero P. M., Bortignon P. F. and Broglia R. A.: Neutino capture cross sections for ^{40}Ar and β-decay of ^{40}Ti. Phys. Lett. **B 345**, 343 (1995).

Honkanen A., Dendooven P., Huhta M., Lhersonneau G., Lipas P. O. Oinonen M., Parmonen J.-M., Penttilä H., Peräjärvi K., Siiskonen T. and Äystö: High-resolution study of the beta decay of ^{41}Ti. Nucl. Phys. **A 621**, 689 (1997).

Adachi T. et. al.: High-resolution study of Gamow-Teller transitions from the $T_Z = 1$ nucleus ^{46}Ti to the $T_Z = 0$ nucleus ^{46}V , Phys. Rev. C **73** 024311 (2006).

Petermann I., Martínez-Pinedo G., Langanke K. and Caurier E.: Breaking of the SU(4) limit for the Gamow-Teller strength in N∼Z nuclei. Eur. Phys. J. A. **34**, 319 (2007).

Poves A., Sánchez-Solano J., Caurier E., and Nowacki F.: Shell model study of the isobaric chains A = 50, A = 51 and A = 52. Nucl. Phys. **A 694** 157 (2001).

Lisetskiy A. F. , Gelberg A., Jolos R. V. , Pietralla N. and Brentano P. von: Quasideuteron states with deformed core. Phys. Lett. **B 512** 290 (2001).

Honma M., Otsuka T., Brown B. A. and Mizusaki T.: New effective interaction for pf-shell nuclei and its implications for the stability of the N=Z=28 closed core. Phys. Rev. **C 69**, 034335 (2004).

Ganioğlu et al.: High-resolution study of Gamow-Teller transitions in the ^{47}Ti(^{3}He,t)^{47}V reaction. Phys. Rev. C **87**, 014321 (2013).

Alford W. P., Helmer R. L., Abegg R., Celler A., Frekers D., Green P., Häusser R., Henderson R., Hicks K., Jackson K. P., Jeppesen R., Miller C. A., Trudel A., Vetterli M., Yen S., Pourang R., Watson J., Brown B. A. and Engel J.: Gamow-Teller strength observed in the ^{48}Ti(n,p)^{48}Sc reaction: Implications for the doule beta decay of ^{48}Ca. Nucl. Phys. **A514**, 49 (1990).

Brown B. A.: Nuclear shell models, ed. Vallieres M. and Widenthal B. H. (World Scientific, Singapore) p.42 (1985).

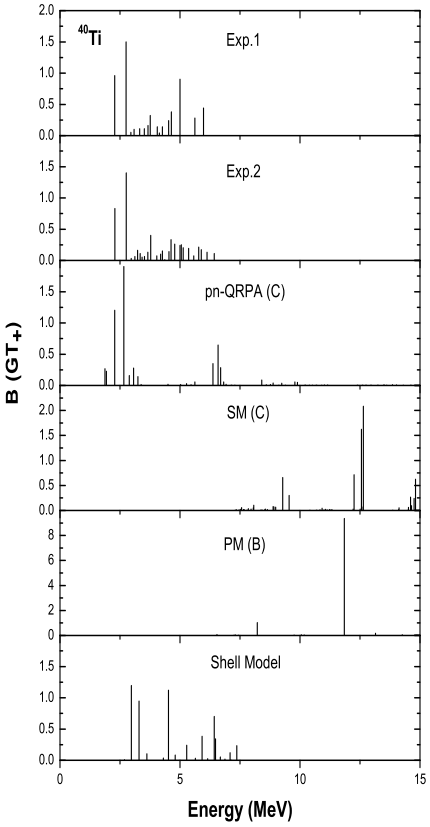

Fig. 1 Comparison of Gamow-Teller (GT_+) strength distributions for ^{40}Ti β decay. Measured data Exp. 1 and Exp. 2 were taken from (55) and (38), respectively. Shell Model results were taken from Ref. (56).

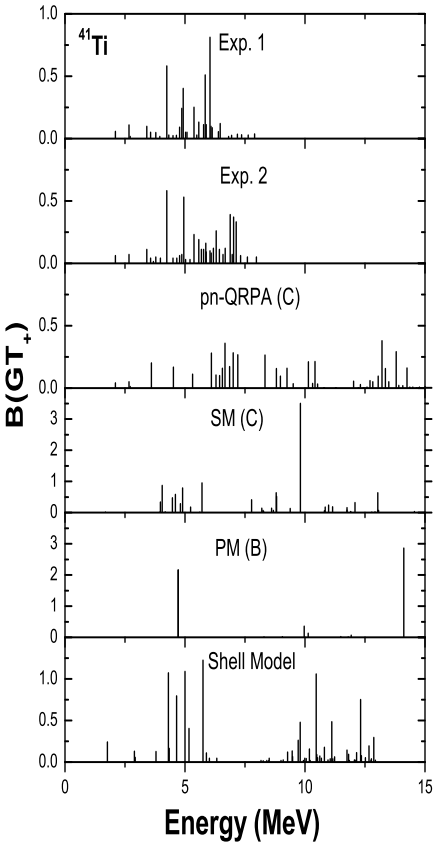

Fig. 2 Comparison of Gamow-Teller (GT_+) strength distributions for ^{41}Ti β decay. Measured data Exp. 1 and Exp. 2 were taken from (57) and (38), respectively. Shell Model results were taken from Ref. (57).

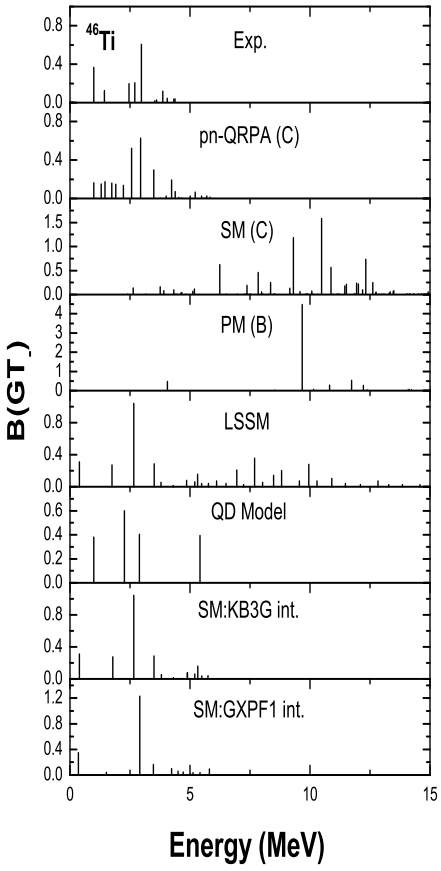

Fig. 3 Comparison of Gamow-Teller (GT_-) strength distributions for ^{46}Ti β-decay. Measured data Exp. was taken from (58). Large Scale Shell Model (LSSM) results were taken from Ref. (59), whereas Shell Model:KB3G int. and Shell Model:GXPF1 int. were taken from Ref. (60) and (62), respectively. Quasi Deutron (QD) model data was taken from Ref. (61).

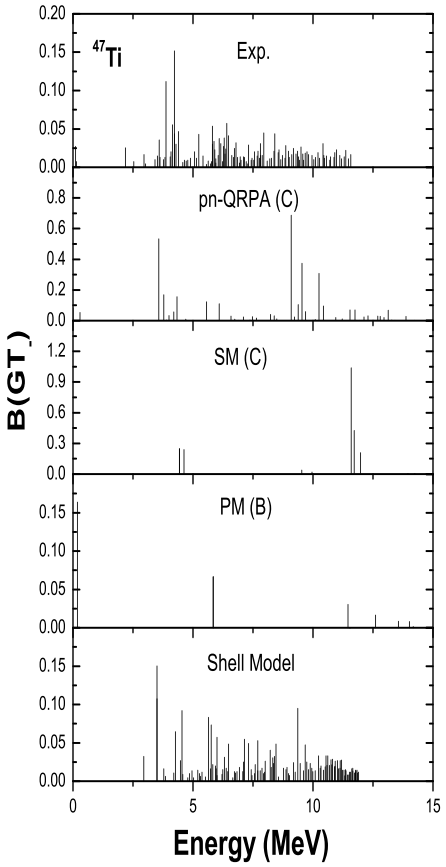

Fig. 4 Comparison of Gamow-Teller (GT_-) strength distributions for ^{47}Ti β-decay. Measured data Exp. was taken from (63). Shell Model results were taken from Ref. (62).

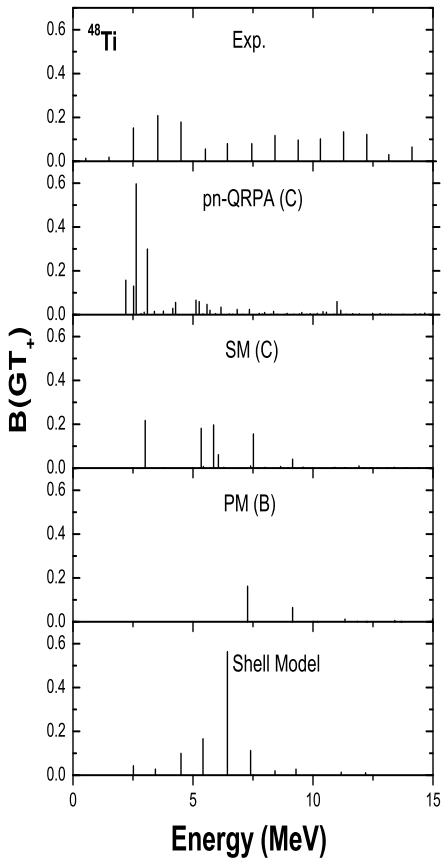

Fig. 5 Comparison of Gamow-Teller (GT_+) strength distributions for ^{48}Ti β-decay. Measured data Exp. was taken from (64) whereas Shell Model (SM) results were taken from Ref. (65).

Table 1 Total GT strengths, centroids and widths of calculated GT strength distribution functions of titanium isotopes, both in electron capture and β-decay directions, for various QRPA models given in first column. For explanation of QRPA models see footnote at the end of Table 1.

^{40}Ti	$\sum$B(GT$_-$)	$\sum$B(GT$_+$)	$\bar{E}_-$	$\bar{E}_+$	Width$_-$	Width$_+$
pn-QRPA (A)[a]	0.78	4.95	6.51	4.16	3.08	2.43
pn-QRPA (B)[b]	0.77	5.05	6.34	3.89	3.01	2.37
pn-QRPA (C)[c]	1.77	6.04	6.41	3.97	3.02	2.37
PM (A)[d]	0.65	13.20	16.49	10.92	7.05	2.29
PM (B)[e]	0.65	11.81	8.94	5.69	7.71	2.97
SM (A)[f]	0.43	11.76	13.57	11.59	9.7	8.25
SM (B)[g]	0.44	11.76	9.48	8.89	7.20	5.94
SM (C)[h]	0.28	9.01	16.48	12.62	4.80	3.01
^{41}Ti						
pn-QRPA (A)	0.68	2.08	9.51	6.65	2.61	2.11
pn-QRPA (B)	0.71	3.45	9.46	9.08	2.61	3.66
pn-QRPA (C)	0.70	4.00	9.54	8.99	2.47	2.74
PM (A)	0.82	5.63	7.58	11.42	4.02	6.08
PM (B)	0.27	8.16	11.82	7.83	10.78	5.37
SM (A)	0.29	7.38	16.86	11.56	10.7	10.82
SM (B)	0.25	7.95	15.83	11.88	9.19	10.54
SM (C)	2.09	12.15	7.02	8.18	4.08	3.03
^{42}Ti						
pn-QRPA (A)	1.25	3.36	5.92	5.63	3.08	3.22
pn-QRPA (B)	1.18	3.32	5.36	5.15	2.95	3.14
pn-QRPA (C)	2.64	4.76	3.47	4.26	2.50	2.88
PM (A)	0.97	5.86	12.18	11.21	4.08	2.01
PM (B)	1.42	7.42	4.57	3.57	4.75	3.31
SM (A)	0.75	6.87	15.65	13.22	7.34	5.58
SM (B)	1.04	7.17	18.59	16.09	9.13	7.82
SM (C)	1.63	7.30	7.73	8.14	4.88	3.45
^{43}Ti						
pn-QRPA (A)	1.17	1.75	10.54	8.58	3.10	3.86
pn-QRPA (B)	1.14	2.59	10.02	8.29	2.98	3.71
pn-QRPA (C)	1.18	2.29	9.87	9.01	2.99	3.62
PM (A)	0.13	0.83	17.36	5.41	6.46	7.11
PM (B)	0.74	0.66	13.86	10.47	7.43	4.46
SM (A)	0.5	7.02	18.87	10.56	7.19	7.40
SM (B)	0.37	7.31	19.73	10.67	8.07	7.24
SM (C)	2.37	6.06	5.06	7.27	2.23	2.81
^{44}Ti						
pn-QRPA (A)	2.60	2.60	5.04	5.13	3.54	3.61
pn-QRPA (B)	1.79	1.76	6.37	6.59	1.90	1.85
pn-QRPA (C)	3.19	3.18	4.62	4.85	3.13	3.24
PM (A)	0.14	0.08	16.25	8.18	6.46	9.55
PM (B)	0.39	0.37	12.24	6.86	8.45	7.88
SM (A)	3.84	3.86	5.61	5.72	3.78	3.72
SM (B)	3.31	3.34	5.78	5.78	3.81	3.48
SM (C)	3.87	3.92	7.94	7.89	3.87	3.99

[a] pn-QRPA (A) are results of spherical pn-QRPA with only ph channel

[b] pn-QRPA (B) are results of spherical pn-QRPA with both ph+pp channels

[c] pn-QRPA (C) are results of deformed pn-QRPA with both ph+pp channels

[d] PM (A) are results of spherical PM with only ph channel

[e] PM (B) are results of spherical PM with both ph+pp channels

[f] SMM (A) are results of spherical (SM) with both ph+pp channels

[g] SM (B) are results of spherical SM with both ph+pp channels

[h] SM(C) are results of deformed SMM with both ph+pp channels

Table 2 Same as Table 1 but for $^{45-50}$Ti.

^{45}Ti	$\sum$B(GT$_-$)	$\sum$B(GT$_+$)	$\bar{E}_-$	$\bar{E}_+$	Width$_-$	Width$_+$
pn-QRPA (A)	3.52	1.25	5.35	10.14	4.25	2.93
pn-QRPA (B)	3.46	1.25	5.25	9.81	4.10	2.80
pn-QRPA (C)	2.59	1.50	7.61	8.83	3.75	3.07
PM (A)	0.39	0.39	1.67	1.82	9.69	3.81
PM (B)	0.43	0.21	2.77	2.03	9.35	4.78
SM (A)	1.23	1.01	7.28	9.16	4.31	5.42
SM (B)	0.93	0.45	7.17	9.54	4.49	6.38
SM (C)	2.72	2.1	8.49	8.58	2.63	1.64
^{46}Ti						
pn-QRPA (A)	4.37	2.07	4.66	5.04	3.41	3.10
pn-QRPA (B)	2.92	1.59	6.24	5.78	1.62	1.87
pn-QRPA (C)	4.48	2.31	4.82	4.11	2.95	3.09
PM (A)	6.81	1.16	5.71	0.44	3.72	2.35
PM (B)	6.55	0.43	6.05	6.44	2.81	6.82
SM (A)	9.20	3.55	8.04	6.14	6.34	5.04
SM (B)	6.64	2.97	6.25	5.01	4.05	3.64
SM (C)	8.60	2.94	10.00	7.42	3.25	3.93
^{47}Ti						
pn-QRPA (A)	3.72	0.40	8.08	8.08	3.65	3.20
pn-QRPA (B)	3.64	0.39	7.73	7.70	3.44	2.97
pn-QRPA (C)	3.63	0.39	7.75	7.70	3.44	2.98
PM (A)	0.34	1.23	2.07	1.38	7.96	4.22
PM (B)	0.38	1.36	3.58	3.04	8.13	4.18
SM (A)	2.79	0.59	12.03	11.35	8.08	8.27
SM (B)	2.61	0.44	9.55	10.19	4.67	6.96
SM (C)	9.16	1.44	8.93	6.38	1.89	1.45
^{48}Ti						
pn-QRPA (A)	6.19	1.84	4.38	4.21	3.25	2.72
pn-QRPA (B)	4.12	1.58	6.10	4.31	1.44	2.11
pn-QRPA (C)	6.12	1.80	5.69	3.57	3.00	2.94
PM (A)	11.71	0.005	2.08	8.96	0.49	5.45
PM (B)	11.85	0.29	2.40	3.08	1.62	5.62
SM (A)	14.10	2.10	7.28	5.83	3.36	1.92
SM (B)	13.86	1.84	7.23	5.57	3.40	1.05
SM (C)	13.85	2.09	12.76	6.42	3.55	4.19
^{49}Ti						
pn-QRPA (A)	3.81	0.31	7.36	6.66	5.06	3.69
pn-QRPA (B)	4.07	0.31	7.20	6.39	4.88	3.46
pn-QRPA (C)	5.59	0.29	7.80	6.72	3.23	2.78
PM (A)	6.93	0.02	10.59	11.27	1.06	7.35
PM (B)	5.29	0.18	10.08	9.13	1.59	6.42
SM (A)	4.22	0.50	9.09	8.02	4.02	3.91
SM (B)	5.17	0.44	8.75	7.56	4.04	3.65
SM (C)	16.00	1.43	12.33	8.06	2.97	1.73
^{50}Ti						
pn-QRPA (A)	8.10	1.64	4.55	3.88	3.40	3.23
pn-QRPA (B)	8.03	1.56	4.28	3.41	3.28	3.04
pn-QRPA (C)	8.01	1.57	5.80	3.86	3.10	3.44
PM (A)	18.75	0.83	5.65	1.47	2.19	1.90
PM (B)	18.60	0.67	5.59	1.96	2.35	4.16
SM (A)	19.66	1.73	8.28	2.40	3.53	1.95
SM (B)	20.01	1.59	8.37	2.16	3.48	1.99
SM (C)	19.13	1.78	14.69	6.45	3.89	4.38

Table 3 Same as Table 1 but for $^{51-56}$Ti.

^{51}Ti	$\sum$B(GT$_-$)	$\sum$B(GT$_+$)	$\bar{E}_-$	$\bar{E}_+$	Width$_-$	Width$_+$
pn-QRPA (A)	8.78	0.27	8.10	7.62	2.93	0.79
pn-QRPA (B)	8.83	0.27	8.07	7.43	2.92	0.78
pn-QRPA (C)	7.90	0.27	8.35	7.29	2.87	1.00
PM (A)	4.99	1.11	9.42	4.80	1.72	1.62
PM (B)	4.67	1.10	9.42	4.34	1.75	2.02
SM (A)	6.44	0.92	11.62	5.56	4.24	1.99
SM (B)	7.08	0.83	13.31	5.19	7.62	1.97
SM (C)	24.61	0.30	13.77	9.51	4.89	6.66
^{52}Ti						
pn-QRPA (A)	10.08	1.52	6.19	3.96	3.25	4.37
pn-QRPA (B)	10.02	1.43	5.96	3.33	3.12	3.89
pn-QRPA (C)	10.01	1.41	6.13	3.31	3.12	3.63
PM (A)	24.67	0.88	8.20	4.64	2.25	2.61
PM (B)	23.45	0.24	7.94	11.45	2.74	6.94
SM (A)	25.40	1.61	14.69	5.22	3.73	4.43
SM (B)	25.21	1.41	14.43	4.17	3.53	2.18
SM (C)	24.73	1.69	16.55	5.82	3.88	4.22
^{53}Ti						
pn-QRPA (A)	9.35	0.14	8.89	6.44	3.20	2.74
pn-QRPA (B)	11.09	0.23	7.00	4.08	3.48	2.16
pn-QRPA (C)	10.00	0.25	7.28	4.50	3.70	2.73
PM (A)	10.55	0.43	8.41	5.03	1.99	2.38
PM (B)	11.89	0.09	7.71	13.09	4.19	7.76
SM (A)	25.40	1.61	14.69	5.22	3.73	4.43
SM (B)	1.96	0.66	9.05	4.57	5.59	2.18
SM (C)	38.71	0.44	13.05	4.61	3.43	3.14
^{54}Ti						
pn-QRPA (A)	12.08	1.40	6.53	2.77	3.20	4.56
pn-QRPA (B)	12.03	1.29	6.26	2.14	3.11	4.03
pn-QRPA (C)	11.96	1.26	6.74	2.43	3.16	4.00
PM (A)	29.93	0.77	7.43	6.16	2.71	3.27
PM (B)	29.00	0.29	7.43	11.54	2.86	6.70
SM (A)	30.99	1.44	16.7	4.85	3.91	5.43
SM (B)	3.81	1.24	16.44	3.54	3.65	2.64
SM (C)	35.14	0.27	20.40	8.87	4.00	6.55
^{55}Ti						
pn-QRPA (A)	9.50	0.13	10.19	5.65	3.27	2.92
pn-QRPA (B)	12.56	0.14	8.05	6.93	4.40	2.49
pn-QRPA (C)	11.35	0.22	7.75	4.04	6.62	4.06
PM (A)	10.08	0.26	9.83	8.42	2.93	3.27
PM (B)	11.16	0.10	7.70	11.77	2.98	6.98
SM (A)	17.62	0.84	17.72	5.16	3.47	3.64
SM (B)	18.21	0.77	17.89	4.52	2.96	2.17
SM (C)	41.96	0.18	13.24	6.01	4.27	3.25
^{56}Ti						
pn-QRPA (A)	13.98	0.88	7.06	2.13	3.43	4.86
pn-QRPA (B)	13.10	0.11	7.30	11.16	2.93	15.08
pn-QRPA (C)	13.49	0.54	7.52	2.85	3.26	4.74
PM (A)	36.89	1.69	6.94	2.29	2.64	3.05
PM (B)	35.95	0.23	6.93	11.69	2.66	5.39
SM (A)	36.32	1.03	18.22	1.92	4.04	2.76
SM (B)	36.17	0.92	18.14	3.10	4.01	7.13
SM (C)	34.45	0.84	19.67	5.72	4.49	5.55

Table 4 Same as Table 1 but for $^{57-60}$Ti.

^{57}Ti	$\sum$B(GT$_-$)	$\sum$B(GT$_+$)	$\bar{E}_-$	$\bar{E}_+$	Width$_-$	Width$_+$
pn-QRPA (A)	14.13	0.11	10.34	4.95	3.59	3.66
pn-QRPA (B)	13.92	0.06	10.10	8.95	3.29	3.00
pn-QRPA (C)	14.23	0.20	7.61	2.33	5.12	3.70
PM (A)	14.15	0.91	10.99	2.68	8.62	2.97
PM(B)	20.78	0.12	7.79	11.86	5.54	5.22
SM (A)	11.5	0.55	18.64	2.34	4.51	2.29
SM (B)	14.40	0.49	19.29	3.00	5.04	5.76
SM (C)	47.48	0.16	15.14	6.64	4.44	3.59
^{58}Ti						
pn-QRPA (A)	15.88	0.71	7.34	2.55	3.81	5.46
pn-QRPA (B)	14.14	0.10	7.91	11.85	3.01	4.90
pn-QRPA (C)	15.65	0.50	7.49	2.55	3.71	5.02
PM (A)	42.09	1.05	6.26	3.39	3.39	4.28
PM (B)	39.29	0.31	6.59	10.76	3.23	4.63
SM (A)	41.47	0.41	18.93	2.72	4.72	4.08
SM (B)	41.33	0.24	18.86	6.14	4.71	7.41
SM (C)	39.05	0.57	20.55	6.92	4.93	6.09
^{59}Ti						
pn-QRPA (A)	15.34	0.06	10.36	5.32	3.87	5.02
pn-QRPA (B)	14.64	0.02	10.64	9.13	3.26	3.33
pn-QRPA (C)	16.70	0.15	7.23	1.54	5.59	3.17
PM (A)	16.49	0.55	8.17	2.93	6.89	3.98
PM (B)	23.73	0.12	6.67	11.39	4.31	4.73
SM (A)	14.17	0.22	18.54	2.23	5.01	3.08
SM (B)	7.87	0.12	19.08	4.53	8.82	6.65
SM (C)	35.81	0.07	15.62	7.93	5.04	3.21
^{60}Ti						
pn-QRPA (A)	17.70	0.50	7.28	3.07	4.03	5.75
pn-QRPA (B)	15.27	0.09	8.15	11.86	3.03	4.35
pn-QRPA (C)	17.67	0.39	7.34	2.85	3.98	5.35
PM (A)	47.59	0.66	5.58	6.20	4.19	4.65
PM (B)	46.53	0.71	5.49	6.86	4.06	5.83
SM (A)	47.03	0.15	19.29	5.65	5.49	5.52
SM (B)	46.92	0.09	19.16	8.76	5.53	6.28
SM (C)	40.69	0.46	20.01	8.28	5.31	6.05

Table 5 Total GT$_-$ strengths and calculated centroids for all GT distribution functions of ^{46}Ti shown in Fig. 3

Panel	$\sum$B(GT$_-$)	$\bar{E}_-$ (MeV)	Cutoff energy in daughter (MeV)
Exp.	1.77	2.53	4.38
pn-QRPA (C)	4.00	4.31	14.84
SM (C)	8.32	9.66	15.99
PM (B)	6.43	9.87	15.06
LSSM	4.17	5.56	15.21
SM:KB3G int.	2.25	2.76	5.76
SM:GXPF1 int.	2.03	2.80	5.96
QD	1.74	2.83	5.42